STEADY-STATE CURRENT FLOW THROUGH GAP JUNCTIONS

Effects on Intracellular Ion Concentrations and Fluid Movement

PETER R. BRINK, RICHARD T. MATHIAS,* STEWART W. JASLOVE, AND GEORGE J. BALDO*
*Department of Anatomy and *Department of Physiology and Biophysics, State University of New York, Stony Brook, New York 11794*

ABSTRACT Double voltage clamp studies were performed on gap junctions contained in septal membranes of the earthworm median giant axon. The gap junctions exhibited no conductance changes in response to voltages imposed across either the septal membrane or the plasma membrane. However, the trans-septal current displayed a slow (10 s) relaxation in response to transjunctional voltage steps. The experimental evidence suggests that this relaxation is a polarization of the septum due to local accumulation/depletion of permeant ions. A theoretical analysis of this observation suggests that the applied electric field causes accumulation of impermeant anions on one side of the junction and depletion on the other, which leads to a change in concentration of permeant ions to maintain macroscopic electroneutrality. The change in concentration of permeant ions generates a transjunctional equilibrium potential that opposes junctional current flow. These results indicate that currents flowing through gap junctions can have an influence on the distribution of intracellular ions. Moreover, the theoretical analysis suggests that such currents will be accompanied by significant intracellular and intercellular water flow.

INTRODUCTION

Many gap junctions display no voltage or time-dependent conductance and have linear current voltage relations (Johnson and Ramon, 1982; Verselis and Brink, 1984, 1986; White et al., 1985; Weingart, 1986; Weidmann, 1970). Linearity is presumably related to the wide diameter and low selectivity of gap junction channels and to the absence of voltage-dependent gating. However, as reviewed below, there are several examples of voltage-dependent gap junctions which change their conductance by gating in response to applied potentials.

Junctions found in early embryos of some fish and amphibians have been shown to depend symmetrically on transjunctional potential. They maximally conduct when coupled cells are at the same potential and close when the potential of either cell is changed (Spray et al., 1981). The gap junctions between the motor and lateral axons of the adult crayfish nerve cord depend asymmetrically on transjunctional potential (Jaslove and Brink, 1986; Furshpan and Potter, 1957). These junctions open when the polarity of the transjunctional potential is in one direction and close when the polarity is reversed, regardless of which cell's potential is changed. A third type of voltage-dependent gating has been described in larval *Chironomous* salivary gland (Obaid et al., 1983). These junctions are controlled by transcellular rather than transjunctional potential. The gap junction channels are open when both cells are hyperpolarized and closed when either cell is depolarized. It is generally believed that voltage-dependent conformational changes in the structure of the gap junction channel underlie these gating processes. The time course of gating is on the order of hundreds of milliseconds for the embryonic and larval junctions, and perhaps two orders of magnitude faster for the crayfish rectifying junctions at room temperature.

In this paper we report another type of electrical regulation of gap junctional current flow. We have found a transjunctional current-dependent current relaxation, which has a time course on the order of tens of seconds. The data suggest that this relaxation is due to accumulation and depletion of ions in the vicinity of the septal junctions. We have tried to identify the physical basis of the accumulation/depletion. Partial differential equations were derived that relate the movement of intracellular ions to fluid flow and intracellular potential. The solutions of these equations were investigated numerically and analytically. We conclude that whenever there is a significant intracellular concentration of ions that are impermeant to gap junctions, steady-state current flow will be accompanied by changes in intracellular ion concentration and fluid movement.

GLOSSARY

Parameters

- a concentration of small intracellular anions, such as chloride or bicarbonate, that are readily permeant to gap junctions (mol/cm^3)
- A concentration of medium-sized intracellular anions that are impermeant to gap junctions yet able to freely diffuse through the cytoplasm (mol/cm^3)
- c concentration of small intracellular cations, primarily potassium plus some sodium, that are readily permeant to gap junctions (mol/cm^3)
- D effective intracellular diffusion coefficient that includes the effects of intracellular organelles, tortuosity, and cytoskeleton (cm^2/s)

$$E = \frac{RT}{Fz}\,\ell n\left[\frac{\text{concentration}(x = 0^+, t)}{\text{concentration}(x = 0^-, t)}\right],$$

transjunctional equilibrium potential (volts)

- F Faraday's constant (10^5 C/mol)
- g specific membrane conductance (S/cm^2)
- I current density (A/cm^2)
- J flux density (mol/cm^2 s)
- $\ell_{1,2}$ distance from septum to point 1, 2 of voltage clamp, see Fig. 1 (cm)
- ℓ distance between points of voltage clamp (cm)
- L specific membrane hydraulic permeability ([cm/s]/[mol/cm^3])
- Os osmolarity (mol/cm^3)
- Pr concentration of large intracellular anions, such as protein, that are impermeant to gap junctions and do not freely diffuse through cytoplasm (mol/cm^3)
- r axon radius (cm)
- R effective resistivity (Ωcm)
- RT/F constant (25×10^{-3} V)
- t time (s)
- u water flow velocity (cm/s)
- V_i/V_T volume of intracellular space per unit volume of tissue
- x longitudinal distance from the septum (cm)
- $\bar{z}$ magnitude of the average valence
- ψ intracellular voltage (V)
- $\psi_{1,2}$ intracellular voltage at points 1, 2 of voltage clamp, see Fig. 1 (V)
- $\Delta\psi = \psi_1 - \psi_2$ (V)
- τ approximate time constant for the current relaxation (s)

Subscripts

- a intracellular anions permeant to junction
- A intracellular anions impermeant to junction
- c intracellular cations
- i intracellular
- j junctional membrane
- m axon surface membrane
- o outside of axon in bath
- p intracellular protein

METHODS

Septal junctions of earthworm median giant axons were studied using the double voltage clamp technique (Spray et al., 1981). Fig. 1 is a schematic representation of the experimental set-up. Axons were impaled with four microelectrodes over an 800-μm distance. Because of the long length constant relative to the distance over which the microelectrodes are placed, accurate voltage control across the junctional membranes was achieved once the clamps had settled (2–5 ms). A fifth microelectrode filled with dye was inserted into the axon some 200–300 μm beyond the voltage clamp electrodes. This allowed introduction of a probe to determine the existence and position of junctional septa. Dye was iontophoretically injected into the fiber as described by Brink and Ramanan (1985). Immediately after the injection, the intracellular concentration of the dye was typically 500–1,000 μM as determined by the methods of Brink (1983). The dyes used were carboxyfluorescein (CFL) or fluorescein sulfonate (FL-S) (Molecular Probes Inc., Eugene, OR).

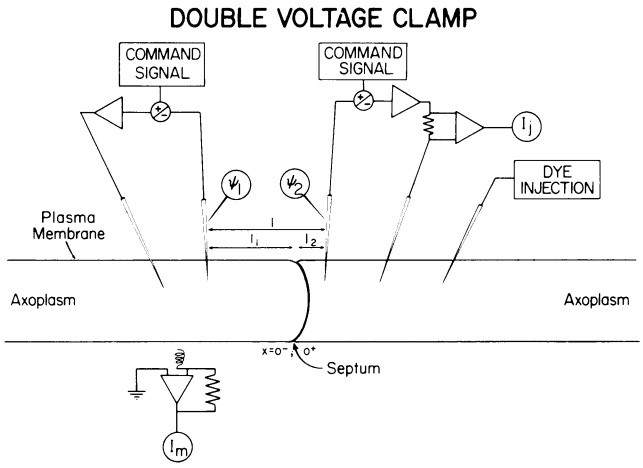

FIGURE 1 The septate giant axon is composed of cylindrical cells, each ~1 mm in length with a diameter of ~80–100 μm. The individual cells are connected to each other end to end. The connections, called septa, contain gap junctions. Four microelectrodes are positioned with two on either side of a septum. The electrodes closest to each side of a septum are the voltage sensing electrodes (ψ_1 and ψ_2) while the other two act as current passing electrodes. A fifth electrode is placed farther away from the septum (800–1,000 μm) and is used to inject fluorescent probes. I_j represents the current which flows through the septum, and I_m represents the current flowing through nonjunctional pathways. The distances between the voltage sensing electrodes are represented by ℓ_1 and ℓ_2.

Under voltage clamp, when no current pulses were applied to inject dye, the voltage recorded by the fifth microelectrode was never >10–20% different from the command potential, confirming that the length constant was in the 3-mm range. The cable equation (Katz, 1966) predicts that ψ_m would be reduced 15% over a distance of 500 μm when the length constant is 3 mm. During dye injection, the response of the four microelectrodes to the current pulses (20–50 nA, 100 ms duration) was observed, thereby allowing a more accurate calculation of the length constant for each individual experiment. For the 63 experiments done in this fashion, the length constant ranged from 1.6 to 4.5 mm with an average value of 3.2 mm.

Before introduction of the dye, a current-voltage curve for the septum was recorded. In all cases the holding potentials before and after a 500-ms test pulse were equal. In addition, long voltage steps (10–60 s) were employed. In some cases the long steps were followed immediately by steps of equal amplitude but opposite polarity.

Under voltage clamp, nonjunctional current (I_m) from the axon was measured by a virtual ground current monitor in the bath. The input resistance of the axons ($[\psi_1 - \psi_2]/I_m$, where I_m = nonjunctional current and ψ_2 is set to the resting potential) was 0.5–1.5 MΩ, which is in close agreement with previously reported values (Dierolf and Brink, 1973).

The four signals (ψ_1, ψ_2, I_j, I_m) were digitized by an A/D converter (Data Translation DT 2801-A) and recorded using an IBM-PC. Earthworms were maintained as previously described (Brink and Ramanan, 1985). Dissection of nerve cords was like that of Brink and Barr (1977). All experiments were performed in either NaCl saline (Brink and

Ramanan, 1985) or acetate saline (Verselis and Brink, 1984) at room temperature (20°C). The saline pH was 7.4.

Numerical Analysis

The general procedure for solving the nonlinear, partial differential equations of the Theory section was to replace first and second derivatives with first and second order difference equations, then solve for each function at time $t + \Delta t$ in terms of the values of all functions at time t. We tested for convergence by running computer simulations with decreasing values of Δt and Δx until the step size did not affect the results.

Eqs. 1–3 were combined using Eq. 13 for electroneutrality to eliminate time derivatives and water flow. This yielded a second order, nonlinear ordinary differential equation relating voltage and the various ion concentrations. Discretizing this equation produced a vector equation of the following form:

$$\mathbf{\Phi}_0\psi = \mathbf{B}_0.$$

If the axon is divided into 2N x-segments, the vector ψ is of dimension 2N with its k^{th} element from the center representing $\psi(k\Delta x, t)$. The matrix $\mathbf{\Phi}_0$ contains the ion concentrations and coefficients of the original differential equation; the vector $\mathbf{B}_0$ contains the ion concentrations and the boundary conditions on ψ at $x = \pm\ell/2$ and $x = 0^{\pm}$.

Each of the ion concentration equations were discretized and equations of the following form resulted.

$$\mathbf{A}(t + \Delta t) = \mathbf{A}(t) + \Delta t[\mathbf{\Phi}_1\mathbf{A}(t) - \mathbf{B}_1(t)],$$

where the vector $\mathbf{A}(t)$ represents the concentration of $\mathbf{A}(x, t)$ at the locations $k\Delta$x, the matrix $\mathbf{\Phi}_1$ contains the voltage, the water flow and the coefficients of the differential equation in x, and the vector $\mathbf{B}$ contains boundary conditions at $x = \pm\ell/2$ and $x = 0^{\pm}$.

The water flow velocity was calculated from

$$\mathbf{\Phi}_3\mathbf{u} = \mathbf{B}_3$$

where the definitions of $\mathbf{\Phi}_3$, $\mathbf{u}$, and $\mathbf{B}_3$ are equivalent to those for the previous equations.

The simulations were begun by setting the concentrations to their initial, uniform, steady-state values, setting $\mathbf{u}(x, 0) = 0$, then solving the voltage equation with the boundary conditions $\psi(\pm\ell/2, 0) = \pm\Delta\psi/2$. The resulting voltage distribution was used in the ion accumulation/depletion equations to solve for the concentrations at $t = \Delta t$. These concentrations were used to calculate the water flow at $t = \Delta t$, then the concentrations were used to obtain the voltage distribution at $t = \Delta t$, and so on.

The simulations were run on an IBM PC-AT with a 32-bit coprocessor (Definicon Systems, Westlake Village, CA). Typically, the axon was divided into 20 segments of length $\Delta x = 4$ μm, and a time interval of Δt = 0.1 s was used. A simulation of concentration changes occurring over a 40-s time span required ~2 min of computer time.

EXPERIMENTAL RESULTS

Current-Voltage Relationship: Short Steps

In response to short (500 ms) voltage steps, the conductance of the septal junctions showed no pronounced transjunctional (Fig. 2 *A*) or plasma membrane voltage sensitivity (Fig. 2 *B*). However, the junctional membrane currents (I_j) decayed slightly with time. This relaxation (Fig. 2) is much like that shown by Johnston and Ramon (1982) for the septal membranes of the lateral giant axons of crayfish. The nonjunctional current for Fig. 2, *A* and *B*, indicate that the input resistances of the two preparations were 650 and 840 KΩ, respectively. The longitudinal resistances (septum in series with axoplasm) were 120 and

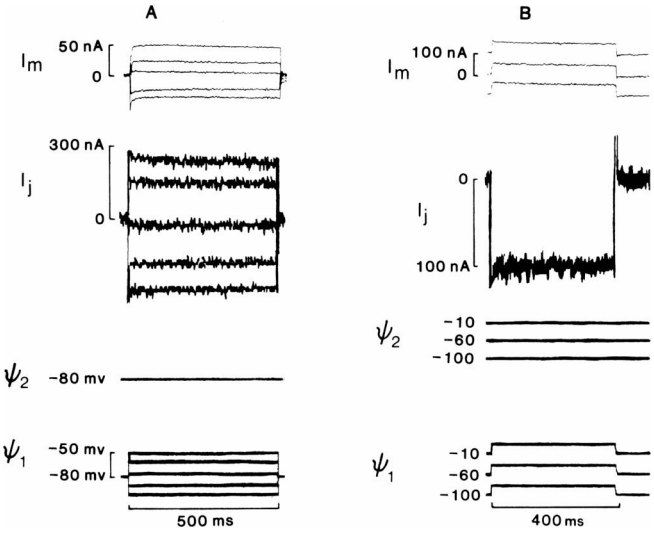

FIGURE 2 (*A*) 500-ms duration clamp steps where I_j shows the junctional membrane current flow and I_m is the nonjunctional current flow. Voltage steps were applied in cell 1 and the holding potential in cell 2 was held constant at −80 mV. Transjunctional voltage was varied over a 60-mV range. The junctional current shows a slight relaxation, even with a short step of 500 ms, but shows no other voltage-dependent behavior. (*B*) Over plotted current traces recorded when the plasma membrane potential was changed over a 90-mV range in both cells. A 400-ms duration step was applied to cell 1 to measure junctional current at the different holding potentials. No change in I_j was observed. The data in *A* and *B* are from two different experiments.

110 KΩ, respectively. The distance between voltage recording electrodes was ~300 μm in both cases and the average axon diameter was 90 μm. Therefore, the resistance of the septum was in the 40–60 KΩ range for both preparations, assuming an axoplasmic resistance of 150 Ω-cm. No attempt was made to compensate for the series resistance contributed by the axoplasm.

Long Steps

The effects of long duration command steps on junctional membrane current are shown in Fig. 3 *a*. With steps of 10 s or longer, a pronounced relaxation, or droop, was noticeable in I_j. Nonjunctional current (shown in upper panel) was for the most part linear, however, in some cases rectification in the hyperpolarizing direction was observed. Immediately after a long step, when the transjunctional voltage was returned to $\psi_j = 0$, junctional current of opposite polarity flowed without the driving force of an applied step. One possibility is that the junctional current is affected by ion accumulation/depletion, established during the applied step. As the ions return to their steady-state distribution, the current declines in time as a consequence of the decay of the transjunctional equilibrium potential. A single current trace is shown (insert, Fig. 3 *a*) to better illustrate the current flow in the presence and absence of an applied step. The line drawn through the 0 current level emphasizes the junctional current flow in the absence of an applied step. The relaxation of I_j, either with or without a

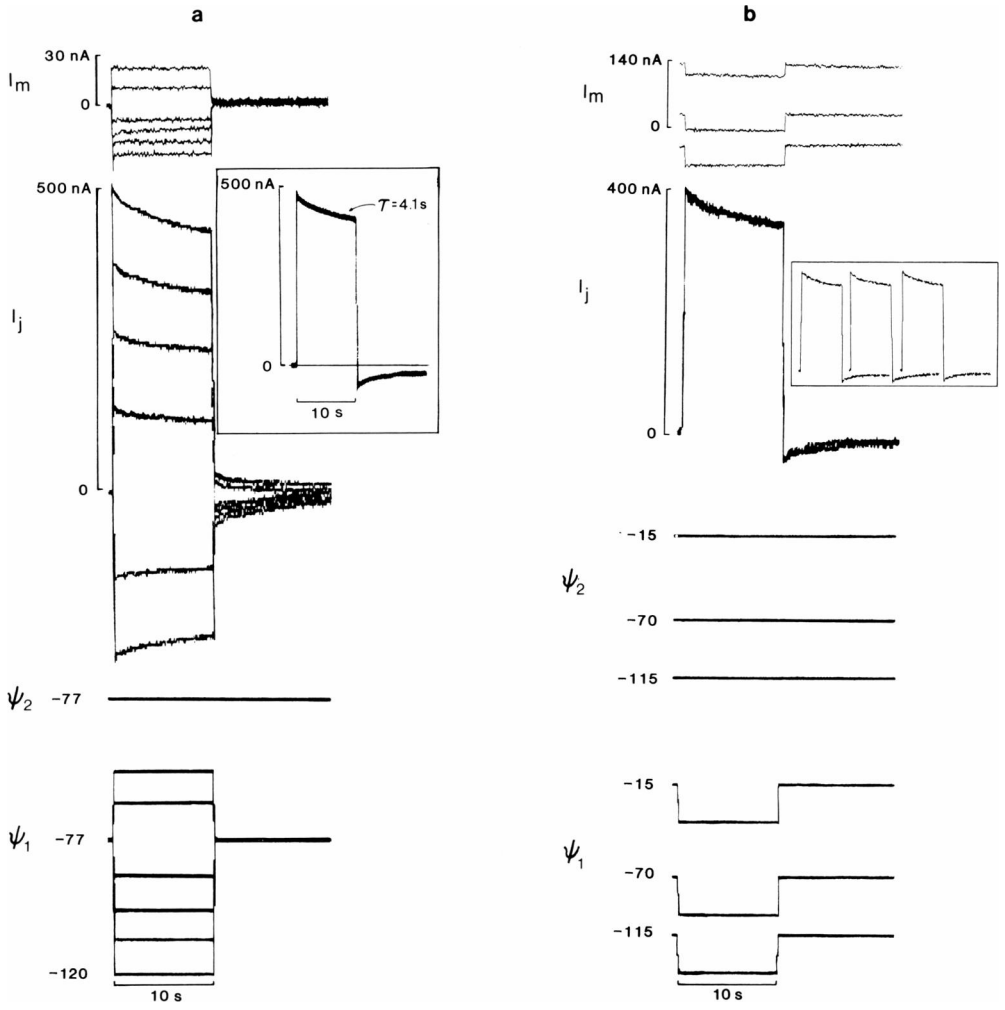

FIGURE 3 (*a*) The same experimental procedure was performed as in Fig. 2 *A* but the duration of the step was 10 s. The step range was again 60 mV in cell 1. Note the pronounced relaxation of I_j. When transjunctional potential was returned to 0 after the 10-s step, there was a relaxation in current of opposite sign to the relaxation during the step. The insert shows a single record to demonstrate the relaxations more clearly. (*b*) The same procedure as Fig 2 *B* was performed but again 10-s steps were used. I_j was unchanged over a 100-mV range of holding potentials. The insert (*b*) shows the individual I_j records for the three holding potentials employed. The experiments of *a* and *b* are from two different axons. The axon was bathed in acetate saline for this experiment.

voltage step, can be approximately fit by a single exponential. The single exponential function used to fit the data had the following form.

$$I_j(t) = (I_0 - I_\infty)e^{-t/\tau} + I_\infty,$$

where I_0 is the instantaneous current and I_∞ is the magnitude of I_j at time $t \rightarrow \infty$. In the case illustrated in Fig. 3 *a* (insert), τ = 4.1 s and the relaxation $(I_0 - I_\infty)/I_0$, is 12%. The relaxation ranged from 5 to 15% and the time constant ranged from 3 to 6 s in 21 experiments.

The plasma membrane potential also had no effect on junctional membrane current during long duration steps (10 s or greater, Fig. 3 *b*). Neither the magnitude nor the time constant of relaxation were significantly affected by holding potential, an observation consistent with ion accumulation/depletion. The insert in Fig. 3 *b* shows junctional membrane current at holding potentials of −15, −70, and −115 mV, left to right, respectively. In all cases the holding potential of the two clamps was set such that $\Delta\psi$ = 0 before and after the application of a command step(s).

The relaxation in current could be a consequence of polarization effects at the septum, or originate within the clamp. To determine whether or not the effects were biological or technical, the clamp electrodes were positioned in a segment of axon with no intervening septum, and the current flowing between the two clamps (I_i) was recorded. The data from two experiments, one with a septum and one without, are compared in Fig. 4. Note that the junctional membrane current in Fig. 4 *a* shows a relaxation much like that of Fig. 3. The steady-state longitudinal resistance was 126 KΩ (effective R_i = 260 Ω-cm). In Fig. 4 *b*, axoplasm lies between the two clamps and the longitudinal current shows no relaxation during an applied step. The total longitudinal resistance was 75 KΩ, which is equivalent to R_i = 157 Ω-cm for a 90-μm diameter axon. In total, 27 double clamps of axoplasm with no intervening septum were performed. In all cases I_i showed no relaxation.

In Fig. 5, as in Fig. 4, one step is applied and followed by a step of equal amplitude but opposite polarity. The currents of the first and second steps have been plotted as absolute values and then superimposed to illustrate the exaggeration of the relaxation for the second step. The relaxation of I_j for the second step is always greater than that of the preceding step regardless of the sequence of the polarities. The relaxation in current of the first step in Fig.

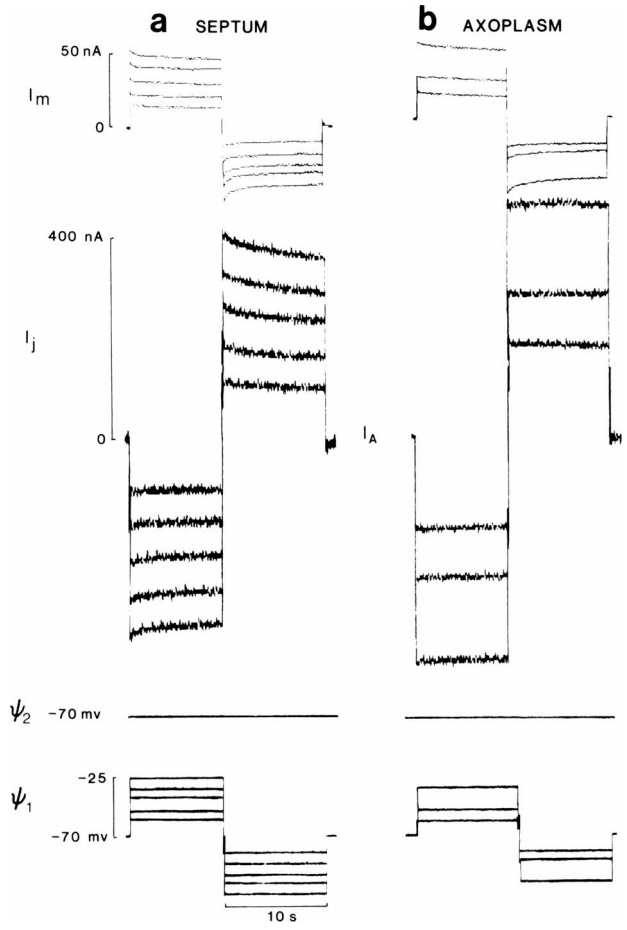

FIGURE 4 Two clamps records are displayed. The first illustrates the clamp with a septum between the two voltage clamps. The step regimen was as follows. A 10-s step was applied, followed immediately by a step of equal but opposite sign. The records show the relaxation of I_j. Regardless of polarity, the second step always showed a more exaggerated relaxation than the first. Voltage clamp of an axon segment with no septum between voltage sensing electrodes produced longitudinal currents (I_i) with no relaxation. The voltage steps ranged over 90 mV for the septum preparation and 70 mV for the axoplasmic preparation. The distance between voltage sensing electrodes was 400 μm for both experiments shown. The lack of relaxation for the axoplasm clamp demonstrates that the relaxation found with the septal preparations is associated with the septa rather than the microelectrodes.

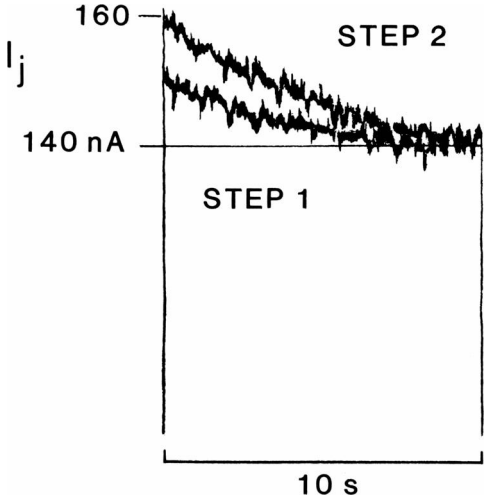

FIGURE 5 A step sequence like that of Fig. 4 was employed to generate the junctional membrane currents displayed. The current from the second step (of equal size but opposite polarity to that of the first step) is shown superimposed on the first with the sign reversed. Regardless of the sequence of polarities, the relaxation of I_j during the second step was always exaggerated relative to the first. The current with the initial value of 160 nA was the junctional current generated in response to the second step. The relaxation is approximately twice the first because the relaxation of I_j for the first step has been superimposed on the relaxation of I_j for the second step. Step duration was 10 s.

5 is 7% of the initial value whereas that of the second step is 14%. The initial current was 150 nA for the first step and 160 nA for the second. The relaxations were fit with a single exponential and the time constant for both was 6 s. This phenomenon was observed in all experiments when a septum was clamped with the two-step regime.

We interpret the increase in the instantaneous current for the second step to reflect the flow of permeant ions that accumulated on one side of the septum during the previously applied step. If so, one expects the relaxation in a second step of equal amplitude but opposite sign to be about twice the relaxation observed in the first step. This is the observation to within the limits of the current noise in Fig. 5 and in other experiments.

It is possible that charged endogenous solutes, of sufficient size, could cause the relaxation in I_j by transiently occluding the intercellular channels. If this were the case, the second step, regardless of polarity, would be expected to show a reduction in the initial phase of the current relaxation rather than an exaggeration (Fig. 5). In this scenario, the first step would push the solute into the intercellular channels and the second step would initially push it back out of the channels. Junctional membrane conductance should be reduced when such solutes occupy a significant number of intercellular channels, but this was not observed experimentally. The fact that current flows in the absence of driving force immediately after a long step also argues against simple channel block by endogenous solutes.

Because we are hypothesizing that the relaxation in current is due to a change in driving force rather than a change in gating, it was important to directly demonstrate that changes in junctional conductance, if any, could not account for the relaxation. Junctional current is related to conductance and driving force by

$$I_j = g_j(\Delta\psi_j - E_j).$$

If we apply small brief voltage changes, $\delta\psi_j$, on top of the potential $\Delta\psi_j$, then

$$I_j + \partial I_j = g_j[\Delta\psi_j + \partial\psi_j - E_j].$$

If the $\delta\psi_j$ are brief compared to the relaxation time, then no significant changes in either g_j or E_j will be induced by the perturbation, hence we can monitor g_j as a function of time

during the large step by

$$g_j(t) = \partial I_j(t)/\partial \psi_j.$$

If driving force is the primary cause of the relaxation, then the percent change in g_j over the time course of the large step should be much less than the percent relaxation in current, even though small changes in g_j may be induced by the redistribution of ions in the vicinity of the junction. This expectation is realized in Fig. 6, where we can detect no systematic change in g_j during either the on or off phase of a large step that causes a 12% relaxation in I_j. Fig. 6 *B* shows the average conductance as measured from the short pulses superimposed on the long step of Fig. 6 *A*. The standared deviation was never >4% for any measurement. In our model, the depletion of permeant ions on one side of the septum is roughly equal to the accumulation on the other, hence the average concentration of permeant ions within the junction changes very little. Thus, one expects changes in g_j due to ion accumulation/depletion to be quite small and outside of the resolution of our measurement. The results in Fig. 6 are entirely consistent with the idea that ion accumulation/depletion produces a time-dependent change in driving force (E_j) and hence the relaxation in current.

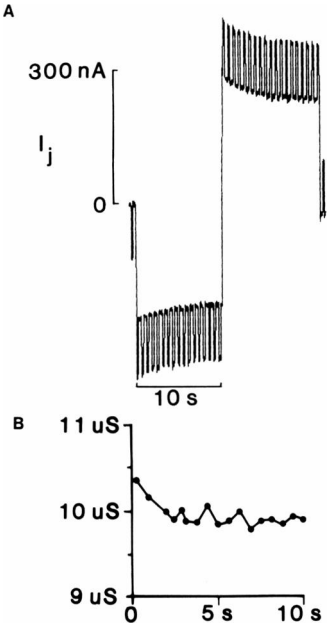

FIGURE 6 (*A*) To determine if conductance changes in the junction were occurring during the relaxation of I_j, short duration steps were superimposed on a long duration step. The first long step was a depolarization of 25 mV (10 s) with short 12-mV steps superimposed. The second long step was a hyperpolarization of 25 mV with short steps of 12 mV superimposed. The short step duration was 225 ms. The amplitude of the short current steps remained constant during the long steps, indicating that there is no conductance change in the junction during the application of the longer steps, and further implicates polarization as the cause of the relaxation. (*B*) The measured conductance of short steps is graphed during the first long step of *A*. The standard deviation for each step was never >4% (i.e., 4 nA when short step average current ≈ 120 nA). For each short step the mean and standard deviation was calculated for the on and off phases of the current. The average conductance was then calculated by subtracting the mean off current from the mean on current and dividing by the step size $\delta\psi$. This procedure gives the total conductance of the junction and axoplasm in series. The standard deviation is calculated from $SD = \sqrt{SD_{ON}^2 + SD_{OFF}^2}/\delta\psi$.

THEORETICAL ANALYSIS

In modeling the intracellular ion fluxes, we assumed that each ionic species moves under the influence of diffusion, conduction, and convection, within the constraint of macroscopic electroneutrality. To produce a relaxation in current that is similar to the experimental observations, we had to assume that the junction is impermeable to some significant fraction of the mobile intracellular anions (or cations, but this seemed unphysiological). The necessity for this assumption can be understood if one considers two different situations. First, imagine that all intracellular anions are immobile and impermeant, whereas cations are mobile and permeant. During a voltage clamp experiment, the mobile cations will migrate to the septum, where their progress is slowed by the junction, thus any accumulation/depletion of cations in the vicinity of the septum would be in the direction to facilitate, rather than diminish, transjunctional current. Second, imagine that anions and cations are in equal concentration, and that they are equally mobile and permeant to the junction. In this situation, both anions and cations would prefer to accumulate/deplete in a direction that facilitates their own transjunctional flux, but to do so, their concentrations would have to change in opposite directions. This cannot happen because of the electroneutrality constraint, hence no accumulation/depletion occurs. By fairly qualitative reasoning, one is therefore led to the conclusion that a significant concentration of relatively mobile yet relatively impermeant anions must be responsible for the relaxation in current. The purpose of the theoretical analysis is to test this qualitative conclusion quantitatively and to show that it can explain the experimental observations. Furthermore, although the experiments are electrical, accumulation/depletion models must include the possibility of water movement, and we conclude from this analysis that significant fluid movement is quite likely to accompany the relaxation in current.

We have considered two models for the experimentally observed accumulation/depletion at the septum. As described above, both models are based on the presence of intracellular anions that are impermeant to the gap junction: the applied electric field moves impermeants in the hyperpolarized cell toward the negative side of the septum and those in the depolarized cell away from the positive side (e.g., Fig. 8). To maintain macroscopic electroneutrality, some permeant ions must also accumulate/deplete, creating transjunctional equilibrium potentials that oppose the junctional current. Moreover, both models predict significant transjunctional water flow induced by the net solute flux across the junction. Net solute flux occurs because the transjunctional cation current exceeds the anion current, thereby creating a net flux of osmotically active solute.

Model 1. In this model we assume that the volume of the axon changes as water crosses the axolemma, thereby keeping the intracellular and extracellular osmolarities

nearly equal. In this situation,

$$A(x, t) + a(x, t) + c(x, t) = \mathrm{Os}_0 \quad \text{osmotic balance}$$

$$A(x, t) + a(x, t) = c(x, t) \quad \text{electroneutrality.}$$

Combining these two equations yields:

$$c(x, t) = \frac{1}{2}\mathrm{Os}_0,$$

or, in other words, the concentration of permeant cations (predominantly potassium) is the same at all locations and at all times. Thus, as the impermeant anions, A, accumulate or deplete in the vicinity of the septum, the permeant anions, a, must do the opposite to maintain electroneutrality.

$$\frac{\partial a}{\partial t} = -\frac{\partial A}{\partial t}.$$

The reduction in total current with time is therefore due to a reduction in the component of current carried by permeant anions.

This model has two flaws. (*a*) It predicts that when permeant anions (chloride and bicarbonate) are washed out of the axon, the relaxation in current should diminish or disappear. However, we incubated axons in Na^+ acetate for 3 h, a procedure presumed to reduce intracellular Cl^- and HCO_3^-. Because acetate is mostly impermeant (~1% is in the permeant protonated form), the cells should then contain essentially no permeant anions. However, no significant change in the relaxation was observed. (*b*) We had to hypothesize an anion junctional conductance that was roughly equal to the cation conductance to duplicate the size of the observed relaxation in current. Because permeant intracellular cations are more numerous than anions, this implies that the junction has significant selectivity for anions over cations, which is not the usual experimental finding (Neyton and Trautmann, 1985).

Model 2. In this model, we assume that osmotic gradients within the axon generate transmembrane water flow, but that the water moves longitudinally along the axon and recrosses the membrane at another location rather than causing a local volume change. In a sense, this treats the axon as a rigid pipe, however, for the longitudinal water flows we expect, the hydrostatic pressures predicted by Poiseuille's equation are on the order of 10^{-7} mm Hg. These pressures are not likely to overcome the compliance of even a very nonrigid membrane/cytoskeletal complex. In this model, the presence or absence of permeant intracellular anions has little effect because they are in relatively low concentration, so consider an axon that contains no permeant anions.

$$A(x, t) + c(x, t) = \mathrm{Os}_i(x, t) \quad \text{total osmolarity}$$

$$A(x, t) = c(x, t) \quad \text{electroneutrality.}$$

Hence

$$\frac{\partial c}{\partial t} = \frac{\partial A}{\partial t},$$

and as the impermeant anions deplete, so do the permeant cations, thereby creating a transjunctional equilibrium potential that opposes cation current flow.

Because model 2 seemed more consistent with experimental observations, we have illustrated some theoretical results from this model. These calculations include complexities not addressed in the above analysis (such as differences in valence or mobility of ions and the presence of multiple ionic species).

Equations

The longitudinal flux of each ion is assumed to obey the Nernst-Planck equation for conduction and diffusion, plus a convection term (Mathias, 1985). We neglect transmembrane ion fluxes across the axolemma in the short segment of axon between the point of voltage control and the septum, because these fluxes are estimated to be <1% of the longitudinal current. However, we include transmembrane water flow, which will be significant if the membranes have a typical hydraulic conductivity. The analysis considers four classes of ions: (*a*) large impermeant proteins that do not move significantly on the time scale of interest but contribute to osmolarity and electroneutrality: (*b*) impermeant anions; (*c*) permeant monovalent anions; and (*d*) permeant monovalent cations. The divergence in longitudinal flux gives the rate of accumulation/depletion (or membrane flux in the case of water).

$$\frac{V_i}{V_T}\frac{\partial A}{\partial t} = D_A\left[\frac{\partial^2 A}{\partial x^2} - \frac{F\bar{z}_A}{RT}\frac{\partial}{\partial x}\left(A\frac{\partial \psi}{\partial x}\right)\right] - \frac{\partial (uA)}{\partial x}, \tag{1}$$

$$\frac{V_i}{V_T}\frac{\partial a}{\partial t} = D_a\left[\frac{\partial^2 a}{\partial x^2} - \frac{F}{RT}\frac{\partial}{\partial x}\left(a\frac{\partial \psi}{\partial x}\right)\right] - \frac{\partial (ua)}{\partial x}, \tag{2}$$

$$\frac{V_i}{V_T}\frac{\partial c}{\partial t} = D_c\left[\frac{\partial^2 c}{\partial x^2} + \frac{F}{RT}\frac{\partial}{\partial x}\left(c\frac{\partial \psi}{\partial x}\right)\right] - \frac{\partial (uc)}{\partial x}, \tag{3}$$

$$\frac{2}{r}L_m(\mathrm{Os}_0 - \mathrm{Os}_i) = -\frac{\partial u}{\partial x}. \tag{4}$$

At the septum ($x = 0^+$ or 0^-, see Fig. 1), the boundary conditions are

$$-D_A\left[\frac{\partial A}{\partial x} - \frac{F\bar{z}_A}{RT}A\frac{\partial \psi}{\partial x}\right] + Au|_{x=0^+} = 0, \tag{5}$$

$$-D_a\left[\frac{\partial a}{\partial x} - \frac{F}{RT}a\frac{\partial \psi}{\partial x}\right] + au|_{x=0^+} = \frac{g_a}{F}[\psi(0^-, t) - \psi(0^+, t) - E_a(t)], \tag{6}$$

$$-D_c\left[\frac{\partial c}{\partial x} - \frac{F}{RT}c\frac{\partial \psi}{\partial x}\right] + cu|_{x=0^+}$$

$$= \frac{g_c}{F}[\psi(0^-, t) - \psi(0^+, t) - E_c(t)], \quad (7)$$

$$u|_{x=0^+} = L_j[\mathrm{Os}_i(0^+, t) - \mathrm{Os}_i(0^-, t)]. \quad (8)$$

The boundary conditions at the points of voltage clamp[1] ($x = \pm\ell/2$ in this symmetric idealization of Fig. 1) and the initial conditions (see Table I) are:

$$A(\pm\ell/2, t) = A_i = A(x, 0), \quad (9)$$

$$a(\pm\ell/2, t) = a_i = a(x, 0) \quad (10)$$

$$c(\pm\ell/2, t) = c_i = c(x, 0), \quad (11)$$

$$\psi_1 = -\psi_2 = \Delta\psi/2. \quad (12)$$

Lastly, we assume that there is some intracellular concentration of larger proteins, *Pr*, of average negative valence, $\bar{z}_p$, whose size and diffusion coefficients ($D_p < 10^{-7}$ cm^2/s) are such that these ions do not move in the time scale relevant to our experiment. Thus, for electroneutrality,

$$\bar{z}_p Pr + \bar{z}_A A + a = c, \quad (13)$$

and the intracellular osmolarity is

$$\mathrm{Os}_i = Pr + A + a + c. \quad (14)$$

Theoretical Results

The solutions to these equations are, of necessity, mostly investigated using numerical techniques (see the Methods section for a description). However, it is possible to derive a few approximate, analytic expressions which are very useful in predicting the effect of various parameters on the ion accumulation/depletion.

Approximate analytic expressions are derived by neglecting water flow (i.e., assume $L_m = L_j = 0$) and neglecting the small concentrations of permeant anions and proteins (i.e., assume $a = Pr = 0$). These assumptions are for convenience and are not physically reasonable; numerical simulations do not include any such assumptions. However, given these assumptions, one can use Eq. 13 in connection with Eqs. 1 and 3 or boundary conditions 5 and 7 to obtain

$$\frac{V_i}{V_T}\frac{\partial \mathrm{Os}_i(x, t)}{\partial t} = D_{eff}\frac{\partial^2 \mathrm{Os}_i(x, t)}{\partial x^2},$$

$$-\frac{\partial \mathrm{Os}_i(0^\pm, t)}{\partial x} = \frac{I_j(t)}{FD_c},$$

$$\mathrm{Os}_i\left(\pm\frac{\ell}{2}, t\right) = \mathrm{Os}_0.$$

Changes in $I_j(t)$ are small in comparison with its initial value, so if we assume $I_j(t) \cong I_j(0)$ these three equations are linear and can be solved to obtain the approximate time course of $\mathrm{Os}_i(0^\pm, t)$. The time constant of solute accumulation/depletion in the vicinity of the septum is approximately

$$\tau = \left(\frac{\ell}{2}\right)^2 \frac{V_i}{V_T}\Big/(3D_{eff}), \quad (15)$$

where the effective diffusion coefficient reflects the constraints of electroneutrality on the movement of both cations and anions

$$D_{eff} = \frac{2D_A D_c}{D_A + D_c}. \quad (16)$$

The steady-state and the initial junctional currents can be exactly derived for these equations. The change in current is approximated by[2]

$$\Delta I_j \equiv \frac{I_j(0) - I_j(\infty)}{I_j(0)} = \frac{1}{2}\frac{g_j \ell R_i D_{eff}/D_c}{1 + g_j \ell R_i}. \quad (17)$$

Eq. 15 predicts that the time constant of the relaxation increases as $(\ell/2)^2$, whereas Eq. 17 predicts that the

TABLE I
PARAMETER VALUES USED IN THE MODEL COMPUTATIONS OF FIGS. 7–9

Initial conditions	Transport parameters	Other parameters
$Pr_i = 20$ mM	$D_a = 1 \times 10^{-5}$ cm^2/s	$V_i/V_T = 0.5$
$\bar{z}_p = 1$	$D_c = 1 \times 10^{-5}$ cm^2/s	$r = 50\ \mu$m
$A_i = 115$ mM	$D_A = 3.5 \times 10^{-6}$ cm^2/s	$\ell_1 = \ell_2 = \ell/2$
$\bar{z}_A = 1$	$R_i = 152\ \Omega$cm	$\ell = 400\ \mu$m
$a_i = 10$ mM	$g_j = 0.32$ S/cm^2	$\psi_1 = -\psi_2 = \Delta\psi/2$
$c_i = 145$ mM	$g_a = 0.02$ S/cm^2	$\Delta\psi = 50$ mV
$\mathrm{Os}_i = 290$ mM	$g_c = 0.30$ S/cm^2	$\Delta x = 22.2\ \mu$m
$\mathrm{Os}_o = 290$ mM	$L_m = 0.15$ cm/s-mOsm	$\Delta t = 0.1$ s
$u = \psi = 0$	$L_j = 0.15$ cm/s-mOsm	$t_{max} = 40$ s

The above values were estimated with the constraint that we measured Os_o, R_i, g_j, and ℓ. Furthermore, the model output was constrained to fit the experimental data.

[1]These boundary conditions are based on the assumption that the volume of axon outside of the region of clamp is sufficiently large to be unaffected by the local concentration changes. This is not precisely true and we have made estimates that the concentrations at $x = \pm\ell/2$ might deviate by ±5–10% from their steady-state values. The direction of these deviations would tend to enhance the gradients. We have not attempted to simulate these effects because the equations become much more complex and the computer time to simulate the concentration changes everywhere in each axonal segment is prohibitive.

[2]This expression includes the approximation that $R_i \simeq 2RT/(F^2 D\ \mathrm{Os}_0)$, which depends on the intracellular cation concentration being approximately ½ Os_0, and the value of $D \gg D_A$.

amplitude of the relaxation increases very little with electrode separation. Though the values of τ and ΔI_j are decreased by water flow, their dependence on other parameters remains valid. In comparing experiments with different electrode separations, we qualitatively verified the dependence on distance, even though the data were from different axons.

Fig. 7 *A* illustrates an overplot of the predictions of the model and experimental data for a step 40 s long. Note that I_j attains a steady-state level within 20 s. The parameters used in the model to generate this curve are listed in Table I. Using the same parameters, Fig. 7 *B* illustrates how the predicted values of τ and ΔI_j vary with water flow. Of course, neither the data nor the model relaxations are simple exponentials, but for small voltage steps the deviations are small so τ is a reasonable measure of the time course. To generate Fig. 8 *B*, we assumed $L_m = L_i$ and repeatedly ran the simulation with increasing values of membrane hydraulic permeability. Increasing water flow tends to sweep away the ion accumulation/depletion at the septum, thus ΔI_j is reduced and steady state is achieved more rapidly (τ is reduced). When the hydraulic permeability exceeds 2×10^{-3} (cm/s)/Osm, there is little further increase in water flow, hence τ and ΔI_j asymptotically approach their minimum values, which are 30–40% of their maximum values at zero water flow. Eqs. 15–17 in connection with Fig. 8 *B* demonstrate various ways in which parameters in the model can be adjusted to fit the data. Thus, the data do not uniquely prescribe the parameters of the model. However, the expressions in Eqs. 15 and 17 are likely to be larger than their experimental counterparts, because water flow reduces both the amount and time course of the relaxation. To fit the data, we chose values of D_A and D_c that seemed physiologically reasonable

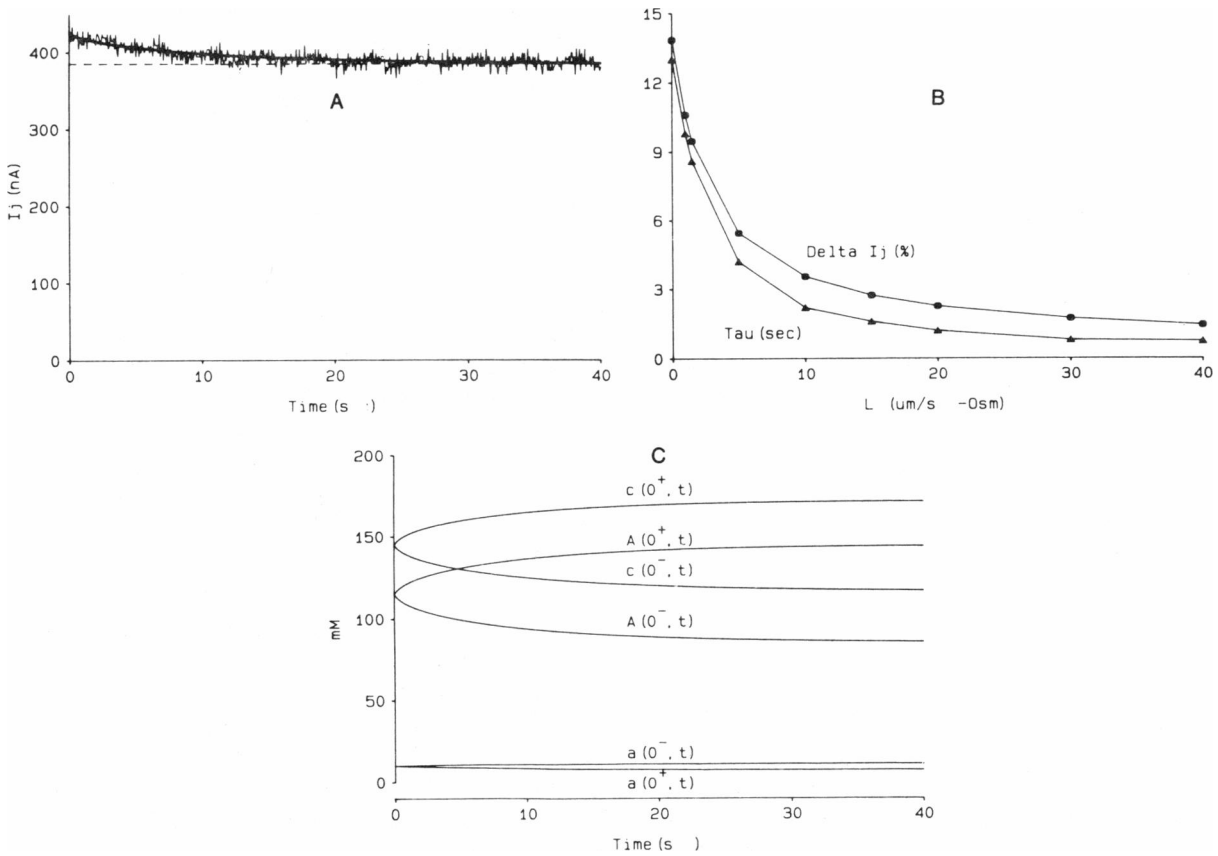

FIGURE 7 Model predictions on the time course of the current relaxation, the effects of water flow, and the time course of intracellular ion accumulation/depletion. (*A*) The experimentally measured current relaxation overplotted with the model output. The duration of the voltage step was 40 s. The straight line was drawn to indicate the final steady state. In this experiment the relaxation, ΔI_j, was 12.2% of the final steady-state current and the estimated time constant, τ, was 6.8 s. (*B*) The predicted effects of increasing water flow on ΔI_j and τ. We used Eqs. 15–17 to choose parameters that produced a value of τ of 13 s and ΔI_j of 14% when there was no water flow. We then allowed there to be some finite membrane hydraulic water permeability ($L_m = L_j = L$) and computed the values of τ and ΔI_j as L was increased. A value of $L = 1.5$ μm/s-Osm produced the best fit of the data shown in panel *A*. In other experiments, values of L ranged from ~1.5–10 μm/s-Osm given our assumed values of D_a, D_c, and D_A. (*C*) The time course of intracellular concentration changes that are predicted to underlie the data presented in panel *A*. The concentrations illustrated are those on either side of the septum ($x = 0^{\pm}$). The impermeant anions, $A(0^{\pm}, t)$, migrate in the applied electric field but cannot cross the junction, hence they accumulate and deplete. The permeant anions, $a(0^{\pm}, t)$, and permeant cations, $c(0^{\pm}, t)$, accumulate and deplete to maintain macroscopic electroneutrality. They create transjunctional equilibrium potentials, given by the Nernst equation, and cause the observed relaxation in current (see Eqs. 6 and 7).

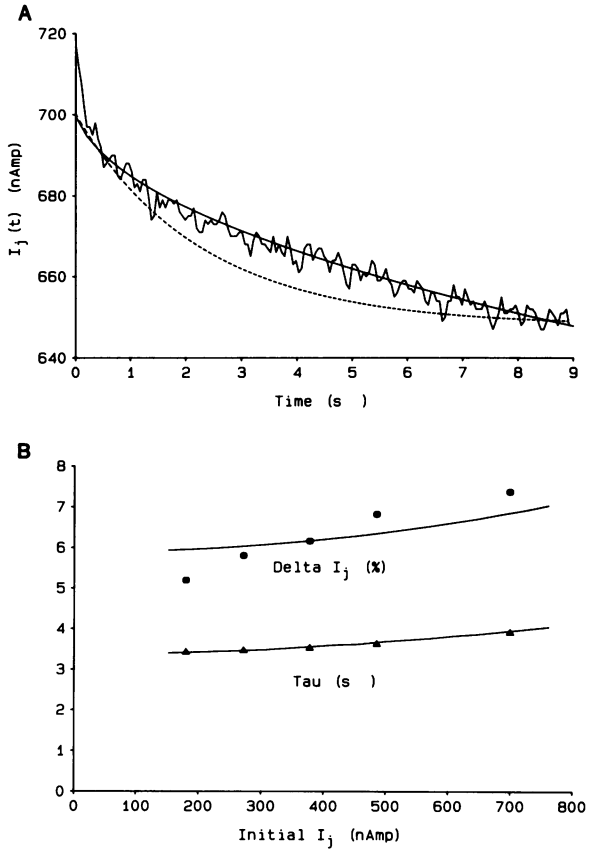

FIGURE 8 A comparison of the experimental and theoretical dependences of τ and $\%\Delta I_j$ on the initial current (or voltage step, because initial current is linearly related to the voltage step). (*A*) shows an expanded view of the current relaxation due to a large (90 mV) step in potential. The initial data points are obscured by the capacity transient, so the best fit of the model (*solid line*) was subject to our estimate of these points. In panel *B*, the $\%\Delta I_j$ is taken from the model fit and therefore includes the same uncertainty. The "time constant" represents the time for 63% of the change in ΔI_j, as estimated by the model curve. The curve in panel *A* represents the data points on the right handside of panel *B*. The dashed line shows an exponential fit that appears to describe ΔI_j accurately, but obviously has the wrong time constant. If the time constant is adjusted, then the endpoints are missed, so for an accurate, quantitative comparison, an exponential fit was not useful. (*B*) The experimentally observed changes in τ and $\%\Delta I_j$ (*points*) overplotted with the model calculations using fixed parameters for various voltage steps. Both the model and the data show a slowing and increase in the relaxation with increasing current. Moreover, the time course becomes decidedly nonexponential for large currents, as shown in panel *A*. These nonlinear effects appear, from the model calculations, to be due to changes in the intracellular resistivity, caused by large changes in intracellular ion concentrations, superimposed on the changes in driving force.

and then adjusted the hydraulic permeabilities until the theory overplotted the data.

One interesting feature of the analysis is that the observed relaxation in current is small relative to the concentration changes needed to produce it. The time course of the concentration changes on both sides of the septum are illustrated in Fig. 7 *C*. The impermeant anions, $A(0^+, t)$, accumulate on the negative potential side (0^+) of the junction because they migrate in the electric field but cannot cross the junction. To maintain electroneutrality, the permeant cations $c(0^+, t)$ also accumulate and the permeant anions $a(0^+, t)$ deplete. The opposite occurs on the positive potential side (0^-) of the junction. The result is a decrease in the driving force for the ionic current crossing the junction and an increase in transjunctional osmotic pressure.

Fig. 9 shows the final, steady-state distributions of intracellular voltage, ions, and water flow corresponding to the current relaxation shown in Fig. 7 *A*. The initial and final voltage profiles are shown in Fig. 9 *A*. The relaxation in current is proportional to the change in voltage gradient; this change is small in comparison with the changes in concentration gradients. In Fig. 9 *B*, the accumulation/depletion of the impermeant anions, *A*, causes the changes in permeant cation and anion concentrations. Because the permeant cations are more numerous, their effect on the current dominates that of permeant anions, so the results are essentially independent of the presence or absence of permeant anions. Nevertheless, the gradients in both $c(x, \infty)$ and $a(x, \infty)$ are in a direction which reduces trans-septal current flow. The longitudinal water flow velocity at steady state is shown in Fig. 9 *C*. This flow is composed of a longitudinal component, which is proportional to the transjunctional osmotic pressure, and a transmembrane flow in the vicinity of the septum, where osmotic gradients have been generated as a result of the accumulation/depletion.

We have no direct experimental evidence for the predicted water flow, but accumulation/depletion must be accompanied by osmotic effects. The actual amount and path (trans-septal vs. transmembrane) of the water movement depends on the hydraulic conductivities. We do not know of any data on the hydraulic conductivity of gap junctions, so we arbitrarily chose $L_m = L_j$ and picked a value that was conservative but physiologically reasonable.

Fig. 8 *A* shows an expanded view of another data set with the model calculation overplotted (*solid line*) and also a simple exponential (*dashed line*). In the model calculation for this and other fits, the same parameters as in Table I were used, except g_j and D_A were adjusted ± 10% to obtain a best fit. This current was in response to a large 90-mV step and one can see that it is noticeably nonexponential, whereas smaller responses were difficult to distinguish from an exponential. The change in current, ΔI_j, is estimated by subtracting the initial and final currents in the curve fit, and the time constant, τ, is taken as the time to 63% of ΔI_j. Both of these values are slightly underestimated because the pulse is only 10 s in duration, however, for the purpose of comparing theoretical and experimental results, we feel this procedure was adequate.

Fig. 8 *B* shows the experimental variation in $\%\Delta I_j$ and τ from experimental data (*points*) and the model (*solid lines*) as a function of initial junctional current. The experimental data points were obtained by curve fitting the

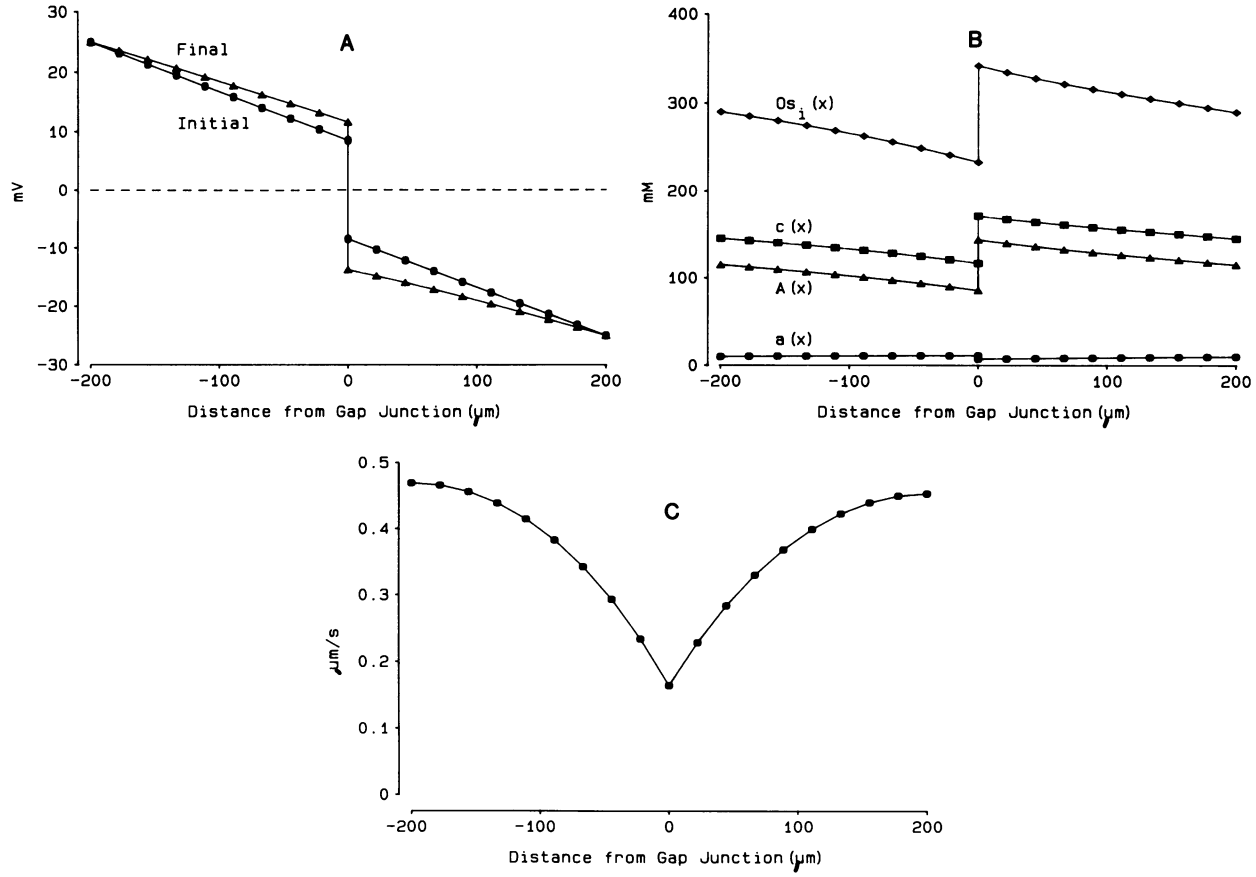

FIGURE 9 Model predictions on the inital and final steady-state distributions of intracellular voltage, ion concentrations, and water flow, (*A*) The initial ($t = 0^+$) and final ($t = \infty$) intracellular voltage as a function of position. The obvious asymmetry occurs because the intracellular resistivity is proportional to the concentration of ions and, as one can see in panel *B*, the concentration (Os_i) is reduced on the left of the septum and increased on the right. If one reverses the polarity of the applied voltage, the asymmetry will reverse leading to symmetrical time courses for current flow. (*B*) The final distributions of intracellular ions. Each concentration was initially equal to its value at $x = \pm 200$ μm at all locations. The concentration of large intracellular anions (*Pr*) is not shown because it is assumed to remain at 20 mM everywhere on this time scale. The concentration gradient of the impermeant anions, $A(x, \infty)$, should facilitate their movement across the septum, however, because the junction will not allow them to pass, the steady-state flux is zero. The gradients in permeant anions, $a(x, \infty)$, and cations, $c(x, \infty)$, are set by the gradient in $A(x, \infty)$ and the requirement for electroneutrality. Each of these gradients is in a direction to oppose the flux of each permeant ion, hence the reduction in current flow with time occurs as these gradients build. (*C*) The final steady-state water flow profile; initially the water flow was zero. The velocities shown represent the movement of 0.02–0.05 μl of fluid per cm^2 of septum every second or, for an axon of 50 μm radius, the flow is 1.6–3.9 pl/s. The maximal flows at $x = \pm 200$ μm are the sum of the trans-septal and transmembrane flows due to the trans-septal concentration gradient and the transmembrane concentration gradient in the vicinity of the septum. The amount of fluid moved varies in proportion to the trans-septal current density so a more physiologically reasonable flow would be at least 1,000 times smaller, which is still a physiologically relevant amount of fluid movement. For example, the renal proximal tubule is a vigorous water transporting tissue yet it reabsorbs fluid at a rate per area of epithelium that is a few hundred times smaller than the flow in panel *C*.

model to obtain a best fit to the observed current responses. This procedure was adopted because a simple exponential was such a poor fit to the large pulses that the value of τ was fairly arbitrary. As one can see in Fig. 8 *A*, the model provides an accurate fit to the data, although the actual initial value of I_j is not easily measured because of the capacity transient. The theoretical lines were computed by fixing the model parameters at their average values from all the curve fits, then varying the voltage command step.

The experimental and theoretical values of both τ and $\%\Delta I_j$ increase somewhat with increased junctional current. In this axon, the experimental change in $\%\Delta I_j$ was large, greater than that predicted by the model, but in other axons the change was less. This variation is a consequence of the nonlinear nature of accumulation/depletion. We are not certain of its exact physical cause, but in the model it seemed to be related to the depletion of ions on one side of the septum. This depletion increased R_i, thereby increasing the $\%\Delta I_j$ beyond what is due to changes in E_j. Moreover, by reducing the current, the time to steady-state is lengthened.

We have examined the effect of model parameters on the time constant and the amount of the relaxation. In summary, we find that the time constant of the relaxation is most sensitive to (*a*) the distance between the clamp and the septum, $\ell/2$ (see Eq. 15), (*b*) the diffusion coefficient,

D_A, for impermeant anions (see Eq. 15), and (*c*) the water flow (see Fig. 7 *B*). The time constant is sped up by decreasing $\ell/2$, increasing D_A, or increasing water flow. Other parameters have little effect on the time constant but can alter the amplitude of the relaxation. For example, increasing the average valence of impermeant anions, $\bar{z}_A$, from 1 to 2 approximately doubles the amplitude of the relaxation but reduces the time constant by only 20%. The amplitude of the relaxation is particularly sensitive to the junction's permeability to the "impermeant" anions. If we assign the "impermeant" anions a junctional permeability that is one tenth that of cations, the amplitude of the relaxation decreases threefold, whereas the time constant decreases only 15%. Thus, the amplitude of the relaxation is sensitive to the following parameters and is decreased by (*a*) decreased D_A, (*b*) increased water flow, (*c*) decreased $\bar{z}_A$, and (*d*) any small junctional permeability for the "impermeant" anions. The parameters listed in Table I could therefore be significantly altered and still produce calculated results that match the experimental findings. However, the order of magnitude of each parameter seems physiologically reasonable so the conclusion is that one should expect accumulation/depletion to occur in the vicinity of the septum.

DISCUSSION

Experimental Results

In summary, the gap junctions of the septal membrane of the earthworm giant axon show no voltage dependence over a range of $\sim \pm 50$mV. Moreover, their conductance does not change with either voltage or current, so endogenous solutes do not act as channel blockers. However, long-term steady currents cause a redistribution of intracellular ions that reduces the transjunctional electrochemical driving force for permeant ions.

We have presented six lines of evidence to support these conclusions. (*a*) The "instantaneous" current voltage relationship is linear. (*b*) Transjunctional current diminishes (relaxes) during long-term voltage clamp steps. The relaxation is 5–15% of the initial current and the apparent time constant is 3–6 s. (*c*) During long-term voltage clamp steps, the slope conductance remains constant. (*d*) Starting from a transjunctional potential of zero, symmetric steps to $\pm\Delta\psi$ yield symmetric currents. (*e*) After a long-term step to either $\pm\Delta\psi$, on return of the transjunctional voltage to zero a relaxation in current is observed that is equal and opposite to that observed in the induced current. (*f*) Stepping from $\pm\Delta\psi$ to $\mp\Delta\psi$ yields asymmetric currents with the relaxation of the second current always being approximately twice that of the first.

Accumulation/depletion of ions reduces the current primarily by changing the driving force rather than the conductance, as described. Moreover, because the two axonal segments are presumed to have the same intracellular composition, equal but opposite voltage steps from zero transjunctional potential should produce symmetric currents. However, because stepping to $+\Delta\psi$ induces a transjunctional equilibrium potential $+E_j$, a step to $-\Delta\psi$ from $+\Delta\psi$ must eliminate the concentration difference that causes $+E_j$ and establish an opposite concentration difference to produce $-E_j$ at steady state. Hence, all of the experimental results described above are consistent with our expectations for ion accumulation/depletion affects on current flow through gap junctions.

Theoretical Analysis

The analysis predicts that there must be a significant intracellular concentration of impermeant ions in order for accumulation/depletion to occur. Because most of the intracellular cations are potassium and sodium, which are freely permeant to gap junctions, we have assumed that it is impermeant anions that lead to the concentration changes in permeant ions.

The septum is the dominant barrier to ion migration in the applied field, therefore, without the constraint of electroneutrality, the tendency for ions to accumulate and deplete near the septum is such that their concentration gradients favor trans-septal migration rather than oppose it. However, this tendency is countered by the requirement of electroneutrality. If all ions are permeant, there can be little change in trans-septal driving force. But if one ionic species is much less permeant than the others, then it accumulates/depletes at the septum to facilitate its own trans-septal migration. The concentrations of other species are then dictated by the requirement for electroneutrality, so they accumulate/deplete in a manner that opposes their own trans-septal migration. Insofar as these other ions carry the majority of the current, we observe a relaxation in current. In order for this relaxation to be significant, there must be a fairly large concentration of anions which have a very small junctional permeability.

Two other interesting conclusions came out of the simulations. First, rather small changes in voltage clamp current reflect significant changes in the intracellular distribution of ions, and second, when trans-septal current flows, water is almost certain to follow. The changes illustrated in Fig. 9 vary approximately linearly with the applied current (see Fig. 8), so in vivo currents will have proportional effects, though such currents are much smaller than those applied during voltate clamp. Thus, in syncytial tissues, steady state in vivo currents will induce intracellular concentration changes, fluid movement and convection of small solutes. For example, in the heart, the wave of depolarization proceeds in the opposite direction to the wave of repolarization, hence the axial current is always in the same direction and a significant average longitudinal current flows that is proportional to the frequency of action potentials. The local concentration changes therefore contain information on the frequency of action potentials and might provide feedback information to the cells. Moreover, steady-state current exist in the lens

(Mathias and Rae, 1985) and they may exist in many other tissues as well. The accompanying convection of solutes may be a means of supplying the metabolic needs of regions of tissue that are not in close proximity to capillaries.

We would like to thank Catherine Garcia and Nancy Walker for their preparation of the manuscript.

This work was supported by National Institutes of Health Projects EY06391, HL36075, GM24905, and HL31299.

Received for publication 6 July 1987 and in final form 30 November 1987.

REFERENCES

Brink, P. R., and L. Barr. 1977. The resistance of the septum of the median giant axon of the earthworm. *J. Gen. Physiol.* 69:517–536.

Brink, P. R. 1983. Effect of deuterium oxide on junctional membrane channel permeability *J. Membr. Biol.* 71:79–87.

Brink, P. R., and S. V. Ramanan. 1985. A model for the diffusion of fluorescent probes in the septate giant axon of earthworm. *Biophys. J.* 48:299–309.

Dierolf, B., and P. R. Brink. 1973. Effects of thermal acclimation on cable constants of earthworm median giant axon. *Comp. Biochem. Physiol. A Comp. Physiol.* 44:401–406.

Fursphan, E. J., and D. D. Potter. 1957. Mechanism of nerve impulse transmission at a crayfish synapse. *Nature (Lond.).* 180:342–343.

Jaslove, S. W., and P. R. Brink. 1986. The mechanism of rectification at the electronic motor giant synapse of the crayfish. *Nature (Lond.).* 323:63–65.

Johnston, M. F., and F. Ramon. 1982. Voltage independence of an electrotonic synapse. *Biophys. J.* 39:115–117.

Katz, B. 1966. Nerve, Muscle and Synapse. McGraw-Hill Book Co., New York.

Mathias, R. T. 1985. Steady state voltages, ion fluxes and volume regulation in syncytial tissues. *Biophys. J.* 48:435–448.

Mathias, R. T., and J. L. Rae. 1985. Transport properties of the lens. *Am. J. Physiol.* 249:C181–C190.

Neyton, J., and A. Trautmann. 1985. Single-channel currents of a intercellular junction. *Nature (Lond.).* 317:331–335.

Obaid, A. L., S. J. Socolar, and B. Rose. 1983. Cell-to-cell channels with two independently regulated gates in series: analysis of junctional conductance by membrane potential, calcium and pH. *J. Membr. Biol.* 73:69–89.

Spray, D. C., A. L. Harris, and M. V. L. Bennett. 1981. Equilibrium properties of a voltage-dependent junctional conductance. *J. Gen. Physiol.* 77:75–94.

Verselis, V., and P. R. Brink. 1984. Voltage clamp of the earthworm septum. *Biophys. J.* 45:147–150.

Verselis, V., and P. R. Brink. 1986. The gap junction channel: its aqueous nature as indicated by deuterium oxide effects. *Biophys. J.* 50:1003–1007.

Weidmann, S. 1970. Electrical constants of trabecular muscle from mammalian heart. *J. Physiol. (Lond.).* 210:1041–1054.

Weingart, R. 1986. Electrical properties of the nexal membrane studied in rat ventricular cell pairs. *J. Physiol. (Lond.).* 310:267–284.

White, R. L., D. C. Spray, A. C. Carvalho, B. A. Whittenberg, and M. V. L. Bennett. 1985. Some electrical and pharmacological properties of gap junctions between isolated rat ventricular myoctes. *Am J. Physiol.* 249:447–455.